The Astrophysical Journal, 788:81 (15pp), 2014 June 10 doi:10.1088/0004-637X/788/1/81

BANYAN. III. RADIAL VELOCITY, ROTATION, AND X-RAY EMISSION OF LOW-MASS STAR CANDIDATES IN NEARBY YOUNG KINEMATIC GROUPS

Lison Malo[1], Étienne Artigau, René Doyon, David Lafrenière, Loïc Albert, and Jonathan Gagné
Département de physique and Observatoire du Mont-Mégantic, Université de Montréal, Montréal,
QC H3C 3J7, Canada; malo@astro.umontreal.ca, doyon@astro.umontreal.ca
Received 2013 November 1; accepted 2014 February 23; published 2014 May 23

ABSTRACT

Based on high-resolution spectra obtained with PHOENIX at Gemini-South, CRIRES at VLT-UT1, and ESPaDOnS at the Canada–France–Hawaii Telescope, we present new measurements of the radial and projected rotational velocities of 219 low-mass stars. The target likely membership was initially established using the Bayesian analysis tool recently presented in Malo et al., taking into account only the position, proper motion, and photometry of the stars to assess their membership probability. In the present study, we include radial velocity as an additional input to our analysis, and in doing so we confirm the high membership probability for 130 candidates: 27 in β Pictoris, 22 in Tucana-Horologium, 25 in Columba, 7 in Carina, 18 in Argus and 18 in AB Doradus, and 13 with an ambiguous membership. Our analysis also confirms the membership of 57 stars proposed in the literature. A subsample of 16 candidates was observed at 3 or more epochs, allowing us to discover 6 new spectroscopic binaries. The fraction of binaries in our sample is 25%, consistent with values in the literature. Of the stars in our sample, 20% show projected rotational velocities ($v \sin i$) higher than 30 km s^{-1} and therefore are considered as fast rotators. A parallax and other youth indicators are still needed to fully confirm the 130 highly probable candidates identified here as new bona fide members. Finally, based on the X-ray emission of bona fide and highly probable group members, we show that for low-mass stars in the 12–120 Myr age range, the X-ray luminosity is an excellent indicator of youth and better than the more traditionally used R_X parameter, the ratio of X-ray to bolometric luminosity.

Key words: solar neighborhood – stars: low-mass – stars: pre-main sequence – techniques: spectroscopic – techniques: spectroscopic

Online-only material: color figures, machine-readable tables

1. INTRODUCTION

The search for young low-mass stars in the solar neighborhood has gained tremendous momentum recently as the youth and intrinsic faintness of these objects make them prime targets for planet searches through high-contrast imaging. This is both because young planetary-mass companions shine brighter and because low-mass stars are less luminous, which loosens the imaging contrast requirements. Finding more young moving group (YMG) members also has intrinsic interest: to refine these YMG characteristics (initial mass function, age, velocities, spatial extent), to complete the solar neighborhood census, and to improve and develop new youth indicators.

As YMG members share common kinematics and span similar age ranges, one can search for overlooked members through a detailed kinematic and photometric analysis of nearby stars. The *Hipparcos* mission, combined with multiple radial velocity (RV) studies (e.g., Anderson & Francis 2012; de Bruijne & Eilers 2012) led to the identification of the most massive members of these groups, but the relatively shallow completeness magnitude ($V = 7$–9) prevented the detection of low-mass members (i.e., later than M5). Assuming that YMG stars follow a typical initial mass function, the vast majority of low-mass members are expected to have gone unnoticed. This led to a number of efforts to extend measurements of proper motion, RV, and parallax to the nearby low-mass dwarfs (e.g., Shkolnik et al. 2012).

Proper motion studies beyond the reach of *Hipparcos* also benefitted greatly from the advent other all-sky surveys (e.g., Lépine & Simon 2009; Zacharias et al. 2013) reaching fainter magnitudes. In particular, infrared proper motions can now be obtained by correlating the *Wide-field Infrared Survey Explorer* (Wright et al. 2010) and Two Micron All Sky Survey (2MASS; Skrutskie et al. 2006) surveys, which is ideally suited to measure proper motions well into the substellar regime (Rodriguez et al. 2013; Gagné et al. 2013). These all-sky photometric surveys have now been supplemented by RV measurements coming from various works. Surveys like the Radial Velocity Experiment (RAVE; Steinmetz et al. 2006; Zwitter et al. 2008) and Sloan Digital Sky Survey (SDSS; York et al. 2000) performed RV measurements on a large sample of stars, while others were focused on old low-mass dwarfs (Delfosse et al. 1998; Jenkins et al. 2009; Chubak et al. 2012; Soubiran et al. 2013). These RV studies are key for studying Galactic dynamics. Finally, and not least, parallax measurements of solar neighborhood stars is spear-headed by the CTIOPI and RECONS group (Riedel et al. 2010, 2011, 2014) and other works (Lépine & Simon 2009; Shkolnik et al. 2012; Liu et al. 2013) focusing on the lowest mass component of the solar neighborhood.

To complete the census of nearby young kinematic group members, kinematics alone is not enough to confirm membership, independent youth indicators are also mandatory to confirm the age of these stars. The high magnetic activity of young stars gives rise to various indicators such as Hα emission, X-ray, and UV (Preibisch & Feigelson 2005; Shkolnik et al. 2011; Rodriguez et al. 2011, 2013). Other spectroscopic indicators include the Li abundance (Mentuch et al. 2008; da Silva et al. 2009) and others like sodium and calcium doublets

[1] Based on observations obtained at the Canada–France–Hawaii Telescope (CFHT) which is operated by the National Research Council of Canada, the Institut National des Sciences de l'Univers of the Centre National de la Recherche Scientique of France, and the University of Hawaii.

(Na: 8183–8195 Å, Ca: 8498–8542 Å) that trace low-surface gravity (Lyo et al. 2004; Slesnick et al. 2006; Mentuch et al. 2008; Shkolnik et al. 2009). Stellar rotation and gyrochronology can also be used for constraining the age of an isolated star through a comparison with young stars in open clusters of known ages such as the Hyades, Pleiades, and IC2391 (Irwin et al. 2011; López-Santiago et al. 2009, 2010; Messina et al. 2010). Recently, Reiners & Mohanty (2012) presented the angular momentum evolution in low-mass stars, which can also be used as a youth indicator. To assess the membership of a given star to the known YMGs, a complete description of these groups is essential: their space velocity, spatial extent, luminosity along with appropriate youth indicators. Based on such YMG descriptions, any given star candidate member of a YMG can have its observational properties (proper motion, RV, absolute magnitude) compared against actual observations.

In the present paper, we present the follow-up of the 130 highly candidate members of young kinematic groups identified or re-identified in a previous paper (Malo et al. 2013, hereafter Paper I). In that paper, we presented an analysis tool (BANYAN[2]) based on Bayesian inference to assess the membership probability of a given low-mass star to nearby YMGs. This analysis has unveiled a large population of potentially new young low-mass stars but those stars cannot be confirmed as bona fide members of their respective association until knowledge of their RV, parallax measurements, and signs of youth are secured. The present work focuses on the radial and projected rotational velocity measurements which were measured through the cross-correlation technique using the infrared and optical domain. The paper is structured as follows. The sample and the observations are presented in Section 2 and data reduction is presented in Section 3. A presentation of the radial and projected rotational velocity measurements follows in Section 4. The identification and confirmation of highly candidate members is described in Sections 5 and 6 is devoted to a discussion of rotation-age and X-ray luminosity relations. Concluding remarks follow in Section 7.

2. SAMPLE AND OBSERVATIONS

A detailed account of our initial search sample has been presented in Paper I. In summary, our original sample of stars show chromospheric X-ray and Hα emissions, and have good I_c photometry and proper motion measurements (<0.2 mag and $>4\sigma$). In Paper I, the I-band photometric data came from several studies. Recently, the UCAC4 (Zacharias et al. 2013) catalog published I-band photometric data from the APASS[3] survey. For this paper, we use an uniform source of I-band photometric data by using APASS-i' instead of DENIS and SDSS-DR8 catalogs, when possible. We transform the APASS-i' magnitude from UCAC4 catalog to I_c using conversion derived from the standards of Landolt (Landolt 2009). The transformation is

$$I_c = i_{\rm APASS} - 0.546 \quad (1)$$

and accurate within 0.05 mag over $0.9 < I_c - J < 2.0$.

Using I-band photometry from the UCAC4 catalog has added 141 stars that were not included in Paper I because the I-band photometry was not available. Our initial sample was thus increased to 920 low-mass (K5V–M5V) stars, 75 of which were previously identified as young stars in the literature. By applying our Bayesian analysis to this extended sample, we found 247 candidate members with a membership probability (P) over 90%, among which 50 were already proposed as candidate members in the literature. These candidates were restricted to the seven closest (<100 pc) and youngest (<100 Myr) comoving groups considered in Paper I: TW Hydrae Association (TWA; de la Reza et al. 1989), β Pictoris Moving Group (βPMG; Zuckerman et al. 2001a), Tucana–Horologium Association (THA; Zuckerman & Webb 2000; Torres et al. 2000), Columba Association (COL; Torres et al. 2008), Carina Association (CAR; Torres et al. 2008), Argus Association (ARG; Makarov & Urban 2000), and AB Doradus Moving Group (ABDMG; Zuckerman & Song 2004).

Table 1
Properties of Radial Velocity Standards

Name of Template	Spectral Type	RV (km s^{-1})	$v \sin i$ (km s^{-1})	Ref.	Instrument
HIP 107345	M1V	2.3 ± 0.5	8.2 ± 0.1	1, 1	PH, CR
HIP 1993	M0Ve	6.4 ± 0.1	7.3 ± 2.3	1, 1	PH, CR
HIP 23309	M0Ve	19.4 ± 0.3	5.8 ± 0.3	1, 1	PH, CR
GJ 806	M3V	-24.7 ± 0.1	1.5	5, 2	ESP
GJ 908	M2V	-71.3 ± 0.1	3.0	5, 2	ESP
GJ 382	M2V	7.9 ± 0.1	<1.8	3, 4	CR, PH, ESP
GJ 447	M4V	-31.1 ± 0.1	<2.5	3, 4	PH
GJ 729	M3Ve	-10.5 ± 0.2	2.5	5, 1	CR
HIP 67155	M2V	15.8 ± 0.1	<1.4	3, 2	CR, ESP
HIP 65859	M0.5V	14.56 ± 0.1	<2.0	3, 2	ESP
HIP 68469	M1V	-25.8 ± 0.1	<2.0	3, 2	ESP

Notes. Instrument: PHOENIX (PH), CRIRES (CR), and ESPaDOnS (ESP).
References. (1) Torres et al. 2006; (2) Jenkins et al. 2009; (3) Nidever et al. 2002; (4) Reiners et al. 2012; (5) de Bruijne & Eilers 2012.

2.1. Observations

As described in Paper I, our statistical analysis yields a membership probability, a prediction of the RV and the most probable statistical distance for each star. Membership confirmation requires both a parallax and RV measurements consistent with prediction of the analysis. Some candidate members listed in Paper I present ambiguous memberships, i.e., they could belong to two or more YMGs; the RVs predicted for those groups differ by a few km s^{-1}. Therefore, high-resolution spectroscopy with accuracy of a few km s^{-1} was required to clarify the membership of ambiguous candidates. Observations were performed using two near-infrared spectrographs, PHOENIX (Hinkle et al. 2003) and CRIRES (Kaeufl et al. 2004), and one optical spectrograph, ESPaDOnS (Donati et al. 2006). In all cases, a set of slowly rotating RV standards were observed to calibrate our measurements. These template observations are summarized in Table 1.

2.1.1. PHOENIX

In 2009 and 2010,[4] PHOENIX at Gemini-South was used with the 0.″34 wide slit in combination with the H6420 order-sorting filter (1.547–1.568 μm) to reach a resolving power of $R \sim 52{,}000$ (4 pixels). This wavelength domain was selected as it is advantageously free of strong terrestrial absorption lines (Mazeh et al. 2002).

[2] Bayesian Analysis for Nearby Young AssociatioNs: www.astro.umontreal.ca/~malo.
[3] www.aavso.org/apass
[4] Gemini ID program: GS-2009A-Q-89, GS-2009B-Q-45, GS-2010A-Q-32, GS-2010B-Q-18, QS-2010B-Q-89.

Table 2
Individual Radial and Projected Rotational Velocity Measurements

Name of star	Date (DDMMYY)	Instrument	RV (km s^{-1})	$v \sin i$ (km s^{-1})
J00240899−6211042	081109	PHOENIX	5.8 ± 0.7	20.7 ± 2.0
J00172353−6645124	260809	PHOENIX	10.8 ± 0.2	6.3 ± 1.8
J00172353−6645124	240910	PHOENIX	10.0 ± 0.5	<8.7
J00171443−7032021	010909	PHOENIX	−4.5 ± 0.4	10.1 ± 3.5
J00171443−7032021	170910	PHOENIX	−2.5 ± 0.6	12.2 ± 2.6

(This table is available in its entirety in a machine-readable form in the online journal. A portion is shown here for guidance regarding its form and content.)

Observations were obtained with a typical ABBA dither pattern along the slit with individual exposures of 60–300 s depending on the target brightness. This observing strategy facilitates the removal of sky emission lines through the subtraction of two consecutive images. Along with each science target observation, a slowly RV standard was observed immediately before or after. We also observed 12 M0–M3V slow rotators, which were used to calibrate measurements of rotational broadening. The typical signal-to-noise ratio (S/N) achieved was respectively 30–50 and 90–120 per spectral pixel for science targets and RV standards. Using that setup, 243 observations of 155 stars were obtained with a S/N sufficient to extract RV measurements with an accuracy better than 1 km s^{-1}.

We also used two archival RV standards (GJ 382 and GJ 447) from the Gemini archive, which were observed during the GS-2002B-Q-11 program with the same setup. The reduction was done using the same method as explained above.

2.1.2. CRIRES

CRIRES was used at VLT-UT1[5] with the 0.″4 and 0.″2 wide slit in the order 36 (1.555 μm), resulting in a resolving power of 50,000 and 80,000, respectively. The dithering strategy and individual exposure times were similar to that used with PHOENIX. Each science program also included observations of RV standards and slow rotators. The achieved S/N was respectively 30–70 and 90–120 per spectral pixel for science targets and RV standards. This observing strategy produced high S/N spectra allowing RV measurements with accuracies better than 1 km s^{-1} for 105 observations of 88 stars.

2.1.3. ESPaDOnS

Starting in 2010, 53 stars were observed with ESPaDOnS, a visible light echelle spectrograph at Canada–France–Hawaii Telescope (CFHT).[6] Observations were done using the "star+sky" mode combined with the "slow" and "normal" CCD readout mode, to get a resolving power of $R \sim 68{,}000$ covering the 3700–10,500 Å spectral domain over 40 grating orders. The total integration time per target was between 5 and 120 minutes.

3. DATA REDUCTION

3.1. Near-infrared Data

The data were reduced in a standard fashion for longslit spectroscopy, using custom IDL routines. The individual nods frames were first dark subtracted and divided by a normalized flat field (only for CRIRES data). For PHOENIX data, flat image contains fringe thus we do not use the flat images. The nods frames were then pair-subtracted, and we forced that dispersion to be perpendicular to the trace by correcting the slit inclination. The one-dimensional (1D) spectrum extraction was obtained from the intensity difference image, where a median Gaussian fitting in the spatial direction was used (in both positive and negative traces). Both the data sets were wavelength-calibrated using five strong OH emission lines (1.5539711, 1.5540945, 1.5545890, 1.5546393, 1.5570159 μm; Rousselot et al. 2000) that encompass the wavelength domain used.

The noise in each spectrum was determined by measuring the pixel-to-pixel scatter along the extracted 1D spectrum. Each spectrum was corrected for the barycentric velocity component of the Earth using the IDL function *baryvel* which is available as part of the astrolib package.[7] For visual binary (VB) stars, we reduced each component by fitting two Gaussian profiles to the trace.

3.2. ESPaDOnS Data

The ESPaDOnS observations were reduced by CFHT using UPENA 1.0, an in-house software that calls the Libre-ESpRIT pipeline (Donati et al. 1997). In the present analysis, we used the processed spectra with the continuum normalized to 1 and automatic wavelength correction from telluric lines.

4. RESULTS

The extracted high-resolution spectra enabled measurement of the science target RV from the observed Doppler shift, and the projected rotational velocity ($v \sin i$) from the width of the absorption lines. All 403 observations were analyzed using the procedure described in Section 4.1. Table 2 summarizes all measurements.

In addition, it was possible to investigate the multiplicity fraction of these stars by classifying them into three categories: (1) VBs (using the acquisition images); (2) SB2; and (3) single-line spectroscopic binaries (SB1).

4.1. Radial and Projected Rotational Velocity Measurements

The RVand projected rotational velocity ($v \sin i$) were measured through a cross-correlation between each individual spectrum and a template. The template consisted in RV standard (see Table 1) convolved with rotational profiles and artificially Doppler shifted. All spectra were effectively re-sampled at equal steps of log λ to properly sample data in equal velocity bins. In artificially broadening standard star spectra, the rotational profiles defined in Gray (1992) were adopted, or more specifically we used the IDL *astrolib* routine *lsf_rotate*. The limb darkening

[5] VLT Period: 087.D-0510, 088.D-0553, 089.D-0592, 091.D-0641.
[6] CFHT program: 11AC13, 11BC08, 11BC99, 12AC23, 12BC24, 13AC23, 13BC33.
[7] idlastro.gsfc.nasa.gov

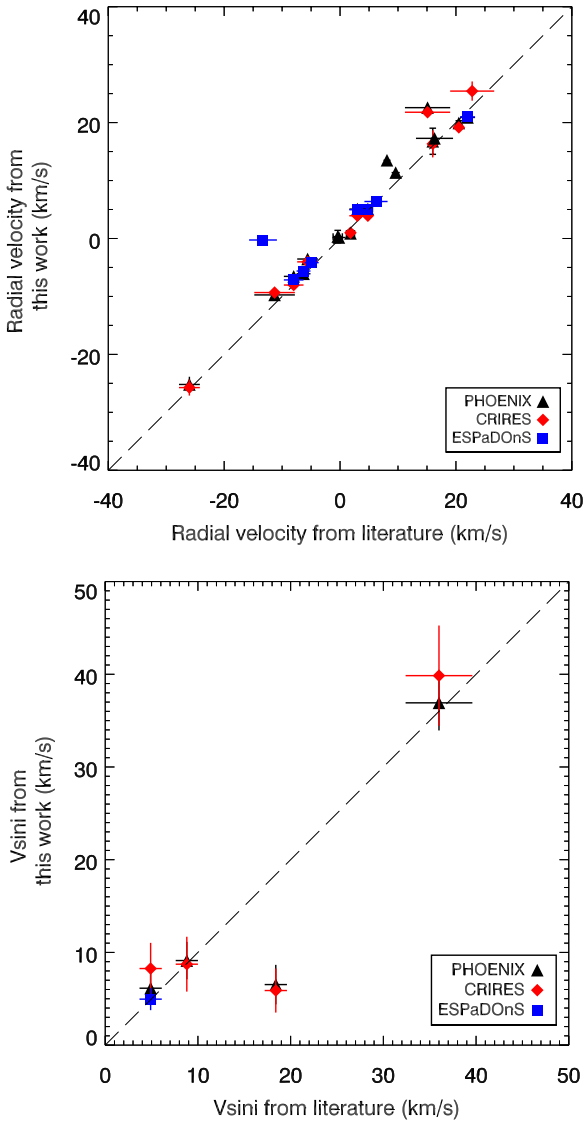

Figure 1. Radial and projected rotational velocity measurements for PHOENIX (black triangles), CRIRES (red diamonds), and ESPaDOnS (blue squares) compared to compiled measurements from the literature. The dotted line illustrates the one-to-one relation between literature and measured velocities.

(A color version of this figure is available in the online journal.)

was set to a typical value of 0.6. The RV and $v \sin i$ parameters were scanned between -150 and 150 km s^{-1} and between 1 and 120 km s^{-1}, respectively. The maximum of the cross-correlation function (CCF) was found by fitting a Gaussian function to the central peak. That yielded the best value of RV and $v \sin i$. For each template, a χ^2 minimization map in two dimension (RV and $v \sin i$) was generated and the template producing the lowest χ^2 was adopted which yielded the final RV and $v \sin i$ measurements.

The wavelengths across which the analysis was performed were the same for all near-infrared data sets (between 1.553 and 1.5575 μm). For the optical data, cross-correlation was performed on an order by order basis between 531 and 793 nm. Only parts of orders devoid of strong telluric absorption were used, these are orders: 26, 27, 28, 29, 30, 31, 33, 35, 36, 37, and 42.

For double-line spectroscopic binary cases, the two peaks seen in the CCF map were both fitted by a Gaussian function.

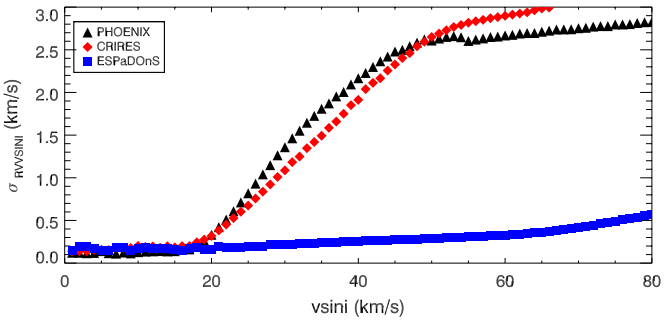

Figure 2. Systematic radial velocity offset induced by the convolution of a slowly rotating RV templates (GJ 382) as a function of $v \sin i$. The CRIRES and PHOENIX data sets (red diamonds, black triangles) show a >1 km s^{-1} systematic errors for $v \sin i$ values above $\sim$30 km s^{-1}, while ESPaDOnS data set (order42: blue squares), which covers a much broader wavelength domain, is almost immune to this effect.

(A color version of this figure is available in the online journal.)

Figure 1 presents a comparison between radial and projected rotational velocity measurements from this analysis and those compiled from the literature. There is an excellent correlation between the literature values and those observed from this work, with a standard deviation of 1.3, 1.9, and 0.8 km s^{-1} for PHOENIX, CRIRES, and ESPaDOnS, respectively. Except for one star (J05332558−5117131), we have similar results for projected rotational velocity measurements. We cannot exclude that this exception is a spectroscopic binary, which was unresolved during our observations but mostly resolved during Torres et al. (2006) observation.

4.1.1. Uncertainty on Radial and Projected Rotational Velocity Measurements

Our sources of uncertainty on RV measurement (similar for $v \sin i$ measurements) fall into three categories, which are expressed in the Equation (2):

$$\sigma_{\rm RV}^2 = \sigma_{\rm noise}^2 + \sigma_{\rm rv\,std}^2 + \sigma_{{\rm rv}\ v\sin i}^2, \quad (2)$$

where $\sigma_{\rm noise}$ is the statistical spectrum noise, $\sigma_{\rm rv\,std}$ is the uncertainty of the RV standard and $\sigma_{{\rm rv}\ v\sin i}$ is the systematic error as a function of $v \sin i$. The $\sigma_{\rm noise}$ was determined by repeating, through a Monte Carlo analysis, the procedure explained in Section 4, this time adding Gaussian noise to each spectral pixel and measuring the standard deviation of the resulting distribution. The second source of uncertainty taken into account is the error on RV and $v \sin i$ of the slowly rotating RV templates, whose values are tabulated in Table 1. The third source is the systematic uncertainty from the RV offset which is effectively measured when comparing RV of an artificially broadened slowly-rotating template to its original self. That RV offset as a function of $v \sin i$ was determined for each template. Figure 2 presents the systematic RV offset as a function of $v \sin i$ when GJ 382 is used as a RV template for the three instruments. The correction is significant for $v \sin i > 30$ km s^{-1}. For example, a target spectrum correlated with that of GJ 382 with a $v \sin i$ of 30 km s^{-1} introduces a systematic RV offset of 1.6 km s^{-1}, 1.1 km s^{-1}, and 0.2 km s^{-1} with PHOENIX, CRIRES, and ESPaDOnS, respectively.

4.2. Multiplicity Fraction

Properties of multiple systems provide strong empirical constraints on star formation theories and evolution. Moreover,

double-lined spectroscopic binaries (SB2) allow precise determination of dynamical properties of the components, including the mass ratio (Gálvez-Ortiz et al. 2010). One clear observational trend, which has gradually emerged is that the multiplicity fraction gradually decreases with decreasing stellar mass (Janson et al. 2012).

During our follow-up program, a sample of hitherto unidentified visual or spectroscopic binaries was uncovered. From the 219 observed stars, we found 37 VB, 12 SB2, and 6 SB1 showing RV variations of more than 5 km s^{-1}. Table 3 lists the properties of the binary systems found within our program.

It is worthwhile to note that for 78% of the βPMG and ABDMG candidate binary systems, our statistical analysis predicted an overluminosity compared to bona fide members. This overluminosity prediction decreases to 33% for THA, COl, CAR, and ARG candidates. As stated in Paper I, this overluminosity could be the result of unresolved binarity. For βPMG and ABDMG, our follow-up observations give credence to our analysis for identifying binary systems.

We find a binary fraction for the low-mass components of 25%, which is consistent with the value published in the literature (25%, 42%; Leinert et al. 1997; Delfosse et al. 2004). Shkolnik et al. (2010) find from a sample of 185 X-ray M dwarfs a spectroscopic binary fraction of 16%. Janson et al. (2012) find a multiplicity fraction for M0V–M5V dwarfs and separations between 0.″08 and 6″ of 27% ± 3%. Bergfors et al. (2010) estimated the multiplicity fraction for young M0V–M6V dwarfs (<600 Myr) with an angular separation 0.″1–6″ to be 32% ± 6%.

We note that ultrafast rotators ($v \sin i$ > 50 km s^{-1}) could be unresolved spectroscopic binaries with two rapidly rotating components. Therefore, a second epoch of measurements is needed to rule out the binary status. An example of such behavior is the TWA candidate member SCR 1425−4113 (see Riedel et al. 2014). While the CRIRES observation did not enable us to detect the two binary components, we measured a $v \sin i$ of 95 km s^{-1}. The second observation with ESPaDOnS enabled us to resolve the two components of the system.

5. CANDIDATES MEMBERSHIP

The statistical analysis presented in Paper I assumed no prior knowledge of the RV information for most systems.[8] The RV obtained in this work can be used to further constraint their membership. Our analysis is based on a kinematical model that takes into account the mean Galactic space velocities (*UVW*) and Galactic positions (*XYZ*) along with their dispersion. Those parameters, given in Paper I, have been slightly modified to take into account several new proposed members from recent studies (Riedel et al. 2014; Shkolnik et al. 2012; Weinberger et al. 2013; Wahhaj et al. 2011). The following stars are considered new bona fide members; in βPMG: 2MASSJ01112542+1526214 (LP 467-16AB), 2MASSJ05064946−2135038 (GJ 3332BC), 2MASSJ05064991−2135091 (GJ 3331A), HIP 23418ABCD, and 2MASSJ03350208+2342356; in TWA: TWA2 and TWA12; and in ABDMG: 2MASSJ06091922−3549311 (CD-35 2722 AB), J07234358+2024588 (BD+20 1790), and HIP 107948. For the sole purpose of establishing the core membership of the association, two outlier stars were removed from the bona fide member list. We removed HIP 51317 (M2V) from the ABDMG bona fide member list because its X-ray luminosity

[8] BANYAN web tool: www.astro.umontreal.ca/∼malo.

Table 3
Properties of Binary Systems

Name (2MASS)	Sep. (″)	$q2/q1$ (Flux Ratio)	Type of Binary[a]	Instr.	Refs.
J00233468+2014282AB	···	···	VB	ESP	1
J00281434−3227556	0.6	0.71	VB	PH	1
J00340843+2523498W	···	···	VB	ESP	5
J01132817−3821024	1.3	0.72	VB	PH	4
J01535076−1459503	2.7	0.80	VB	PH	4
J04480066−5041255A	···	···	VB	PH	1
J05045462−1415337	0.5	0.76	VB	PH	1
J05100488−2340148	1.7	0.63	VB	PH	4
J05100427−2340407A	···	···	VB	PH	4
J05130132−7027418	1.6	0.2	VB	CR	4
J05142736−1514514	2.5	0.3	VB	PH	1
J05241914−1601153AB	···	···	VB	PH	6
J05254166−0909123AB	···	···	VB	PH	7
J05301858−5358483	4.3	0.04	VB	CR	4
J06002304−4401217	1.9	0.97	VB	CR	4
J06153953−8433115	1.1	1.0	VB	CR	1
J06434532−6424396AB	···	···	VB	PH, CR	4
J07105990−5632596	0.9	0.35	VB	PH	1
J07523324−6436308A	···	···	VB	PH	1
J08224744−5726530	8.1	0.2	VB	CR	4
J08412528−5736021	1.4	0.97	VB	PH	4
J08472263−4959574	1.7	0.84	VB	PH	1
J09032434−6348330	7.9	0.11	VB	CR	1
J09423823−6229028	1.3	0.90	VB	CR	4
J10120908−3124451	1.1	0.96	VB	CR	1,3
J11102788−3731520	1.4	0.70	VB+SB2	PH	4
J14142141−1521215	1.3	0.34	VB	PH	1
J16074132−1103073AB	···	···	VB	PH	1
J17104431−5300250A	···	···	VB	PH	1
J17165072−3007104	1.6	0.92	VB	CR	1
J17243644−3152484	0.9	0.74	VB	CR	1
J17494867−4005431A	···	···	VB	PH	1
J18450097−1409053A	···	···	VB	PH	1
J20434114−2433534	1.3	0.98	VB	PH	8
J21103096−2710513	···	···	VB	CR	1
J23002791−2618431	2.1	0.54	VB	PH	1
J23204705−6723209	2.6	0.55	VB	PH	1
Double-line binary					
J01351393−0712517	···	···	SB2	ESP	1
J06131330−2742054	···	···	SB2	PH	3
J07282116+3345127	···	···	SB2	ESP	9
J08185942−7239561	···	···	SB2	CR	1
J08422284−8345248	···	···	SB2	PH, CR	1
J08465879−7246588	···	···	SB2	PH	1
J09361593+3731456	···	···	SB2	ESP	5
J14252913−4113323	···	···	SB2	ESP	1,3
J17462934−0842362	···	···	SB2	PH	1
J18141047−3247344	···	···	VB+SB2	CR	10
J19420065−2104051	···	···	SB2	CR	1
J20100002−2801410	···	···	SB2	ESP	4
Single-line binary					
J01132958−0738088	···	···	SB1	···	4
J02070176−4406380	···	···	SB1	···	1
J02485260−3404246	···	···	SB1	···	1
J15244849−4929473	···	···	SB1	···	1
J18495543−0134087	···	···	SB1	···	1
J22470872−6920447	···	···	SB1	···	1

Notes.
[a] Visual binary (VB), Single-line binary (SB1), Double-line binary (SB2).
References. (1) This work; (2) Torres et al. 2006; (3) Riedel et al. 2014; (4) Janson et al. 2012; (5) Skiff 2010; (6) Bergfors et al. 2010; (7) Daemgen et al. 2007; (8) Shkolnik et al. 2009; (9) Shkolnik et al. 2010; (10) Messina et al. 2010.

Table 4
Main Properties of Young Kinematic Groups

Name of Group	UVW (km s^{-1})	σ_{UVW} (km s^{-1})	XYZ (pc)	σ_{XYZ} (pc)	Number of Objects	Age[a] Range (Myr)	Distance[b] Range (pc)
TW Hydrae (TWA)	−10.53, −18.27, −5.00	3.50, 1.17, 2.15	12.17, −43.23, 21.90	6.14, 7.30, 3.06	12	8–12[c]	42–92
β Pictoris (βPMG)	−11.16, −16.19, −9.27	2.06, 1.32, 1.35	4.35, −5.82, −13.29	31.43, 15.04, 7.56	44	12–22[d]	9–73
Tucana–Horologium (THA)	−9.93, −20.72, −0.89	1.55, 1.79, 1.41	11.80, −20.79, −35.68	18.57, 9.14, 5.29	42	20–40[e]	36–71
Columba (COL)	−12.24, −21.27, −5.56	1.08, 1.22, 0.94	−28.22, −29.74, −28.07	13.68, 23.70, 16.09	20	20–40[e]	35–81
Carina (CAR)	−10.50, −22.36, −5.84	0.99, 0.55, 0.14	15.55, −58.53, −22.95	5.66, 16.69, 2.74	5	20–40[e]	46–88
Argus (ARG)	−21.78, −12.08, −4.52	1.32, 1.97, 0.50	14.60, −24.67, −6.72	18.60, 19.06, 11.43	11	30–50[f]	8–68
AB Doradus (ABDMG)	−7.11, −27.21, −13.82	1.39, 1.31, 2.26	−2.25, 2.93, −15.42	20.10, 18.97, 15.37	48	70–120[g]	11–64
Field stars	−10.92, −13.35, −6.79	23.22, 13.44, 8.97	−0.18, 2.10, 3.27	53.29, 51.29, 50.70	10094		3–150

Notes.
[a] Age range from the literature. Note that relative ages between moving groups are more accurate than absolute ones.
[b] Members with published trigonometric distance only.
[c] Age reference from Webb et al. (1999) and Barrado Y Navascués (2006).
[d] Age reference from βPMG; Song et al. (2003); Makarov (2007).
[e] Age reference from Torres et al. (2001) and Zuckerman & Webb (2000).
[f] Age reference from Torres et al. (2008) and Barrado y Navascués et al. (2004).
[g] Age reference from Mentuch et al. (2008), López-Santiago et al. (2006), and Luhman et al. (2005).

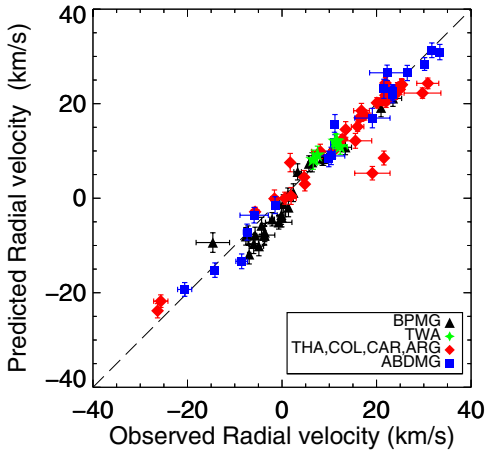

Figure 3. Comparison between predicted and observed radial velocities for the 111 candidate members ($P_v > 90\%$ and excluding known binary).
(A color version of this figure is available in the online journal.)

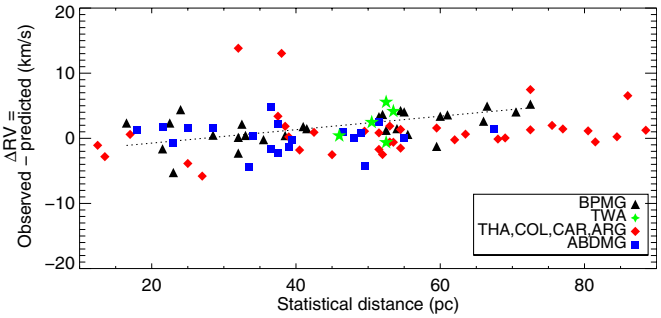

Figure 4. Comparison between predicted and observed radial velocities for YMGs as a function of the statistical distance.
(A color version of this figure is available in the online journal.)

appears to be much more compatible with a field star (see Section 6.2). HIP 24947 in THA was also excluded because it has ambiguous RV measurements (15.2, 23.9 km s^{-1}; Bobylev et al. 2007; Bobylev & Bajkova 2007) that place it either in THA or COL. Table 4 summarizes the main properties of YMGs.

This study presents RV measurements for 368 low-mass stars, of which 202 are new measurements and 166 are compiled from the literature. We also presents $v \sin i$ measurements for 270 stars, of which 202 are new measurements and 68 are compiled from the literature A weighted average of all RV and $v \sin i$ measurements was adopted for stars with multiple measurements (see Tables 5 and 6). Adding the RV information in our Bayesian tool, we found 130 highly probable YMG candidates with membership probabilities (P_v) in excess of 90%. Of these, a subgroup of 117 can be uniquely associated with a single existing YMG, and the remaining 13 have high membership probabilities to 2 or more YMGs. A trigonometric distance is required to assign membership without ambiguity. The 117 candidates are divided the following way between parent YMGs: 27 in βPMG, 22 in THA, 25 in COL, 7 in CAR, 18 in ARG, and 18 in ABDMG. In addition, we confirmed the high membership probability of 57 candidates previously proposed in the literature. Tables 7 and 8 presents the properties of the strong YMG candidates which have a P_v above 90%.

For fast rotators with $v \sin i > 30$ km s^{-1} the RV becomes more uncertain which prevents significant constraints on the membership to be set. However, the rapid rotation deduced from the large $v \sin i$ when combined with other youth indicators (L. Malo et al. in preparation) help constrain the age within certain broad limits (see Section 5.1). Candidates whose membership probability decreases when RV is included in the analysis but have a high projected rotational velocity (>30 km s^{-1}) are tabulated in Table 7.

5.1. Kinematic Model Prediction

As explained in Section 4 of Paper I, predicted RV for candidate members are derived from a kinematic model, using Galactic space velocities of bona fide members as input parameters. One way to assess the accuracy of this model is to look for systematic differences between predicted and observed RV measurements. Figure 3 presents a comparison between predicted and observed RVs for 111 candidate members with $P_v > 90\%$; as expected, the agreement between model predictions and observations is excellent.

For βPMG candidate members, we observe a systematic difference of 3–5 km s^{-1} for a RV range between −10 and 0 km s^{-1}. This systematic difference is also shown in Figure 4 and seem to increase as a function of distance. This may be

Table 5
Compilation of RV from the Literature

Name 2MASS	Spectral Type	RV (km s^{-1})	RV (km s^{-1})	RV (km s^{-1})
J00340843+2523498	K7Ve*	-12.4 ± 2.0[c]	-8.8 ± 0.2[a]	···
J01220441−3337036	K7Ve	4.8 ± 0.8[e]	3.0 ± 1.4[c]	4.7 ± 0.3[a]
J01225093−2439505	M3.5V	9.6 ± 0.7[g]	11.4 ± 0.2[a]	···
J01521830−5950168	M2-3V	8.5 ± 2.3[h]	7.9 ± 1.6[d]	···
J02303239−4342232	K5Ve	16.3 ± 1.1[e]	14.5 ± 2.4[h]	···
J02365171−5203036	M2Ve	16.0 ± 0.1[e]	14.6 ± 2.1[a]	···
J03494535−6730350	K7V	16.3 ± 3.2[h]	16.8 ± 0.2[a]	···
J04435686+3723033	M3Ve	6.2 ± 2.0[c]	6.4 ± 0.2[a]	···
J04480066−5041255	K7Ve(vb)	19.3 ± 0.1[e]	19.2 ± 0.3[a]	···
J05082729−2101444	M5V	22.8 ± 3.8[b]	23.6 ± 1.5[a]	···
J05164586−5410168	M3V	15.1 ± 3.9[h]	21.9 ± 0.4[a]	···
J05254166−0909123	M3.5+M4	28.4 ± 0.5[i]	25.7 ± 0.3[a]	···
J05332558−5117131	K7V	20.5 ± 0.0[e]	19.6 ± 0.4[a]	···
J05335981−0221325	M3V	22.0 ± 1.3[b]	20.9 ± 0.2[a]	···
J11102788−3731520	M4Ve+M4Ve	15.6 ± 0.2[e]	10.2 ± 0.4[a]	···
J11254754−4410267	M4+M4.5	19.5 ± 2.0[l]	20.9 ± 0.8[a]	···
J17292067−5014529	M3Ve	-0.4 ± 0.8[e]	0.3 ± 1.1[a]	···
J18202275−1011131	K5Ve+K7Ve	-13.8 ± 0.8[e]	-9.0 ± 1.0[k]	···
J19102820−2319486	M4V	-8.0 ± 1.7[b]	-6.9 ± 0.3[a]	···
J19233820−4606316	M0V	-0.2 ± 1.1[j]	-0.0 ± 0.3[a]	···
J19312434−2134226	M2.5V	-26.0 ± 1.8[i]	-25.5 ± 1.4[a]	···
J19560438−3207376	M0V	-7.1 ± 2.2[h]	-7.2 ± 0.4[d]	···
J20013718−3313139	M1V	-5.6 ± 1.8[d]	-3.6 ± 0.2[a]	···
J20434114−2433534	M3.7+M4.1	-6.0 ± 0.9[i]	-5.7 ± 0.5[a]	···
J21100535−1919573	M2V	-6.3 ± 1.2[j]	-5.7 ± 0.3[a]	···
J23261069−7323498	M0V(sb)	7.8 ± 1.6[e]	8.9 ± 3.3[a]	···
J23323085−1215513	M0Ve	1.8 ± 0.7[e]	0.9 ± 0.5[a]	···
J23513366+3127229	M2V+L0	-13.5 ± 0.6[f]	-13.6 ± 0.3[a]	···

Notes.
[a] This work.
[b] Binks & Jeffries 2014.
[c] Schlieder et al. 2010.
[d] Kiss et al. 2011
[e] Torres et al. 2006.
[f] Bowler et al. 2012
[g] Bowler et al. 2013
[h] RAVE; Zwitter et al. 2008.
[i] Shkolnik et al. 2012.
[j] Moór et al. 2013
[k] Montes et al. 2001.
[l] Rodriguez et al. 2011.

a hint that the kinematic properties of low-mass members of βPMG differ slightly from that of the bulk population.

5.2. New Bona Fide Members

Although our observations and analysis unveiled 117 new highly probable candidate members to YMGs, a word of caution is necessary before assigning a firm membership to these objects. These candidates will be attributed the status of bona fide members only after their parallax is measured and shown to be consistent with the statistical distance predicted by our analysis. These candidates should also show evidence of youth through other indicators, e.g., lithium EW strength, low-surface gravity, and—as argued in the next section—relatively strong X-ray luminosity.

Recent parallax and RV measurements along with spectroscopic observations provide evidence for adding three new low-mass stars to the list of bona fide members. Those systems are briefly discussed below.

2MASSJ00275035−3233238 (GJ 2006A) and 2MASSJ00275035−3233238 (GJ 2006B). This binary system ($\rho = 18''$, M3.5Ve+M3.5Ve) was first proposed to be a member of βPMG by Riedel et al. (2014) who measured a trigonometric distance of 32.3 ± 1.8 pc, consistent with our predicted statistical distance of 32 ± 2 pc. Its spectrum shows sign of low gravity (hence youth) as evidenced by the strength of the NaI8200 index. Our RV measurements (8.8 ± 0.2 km s^{-1} and 8.5 ± 0.2 km s^{-1}) are consistent with the prediction (8.4 ± 1.5 km s^{-1}) of our kinematic model and yield a very high membership probability in βPMG: $P_v = 99.9\%$ and $P_{v+\pi} = 99.9\%$.

2MASSJ06131330−2742054 (SCR 0613-2742AB). This is another binary system ($\rho = 0\farcs093$, M4V unresolved) proposed to be a member of βPMG by Riedel et al. (2014) at a trigonometric distance of 29.4 ± 0.9 pc, consistent with our statistical distance of 25 ± 6 pc. Our RV (22.5 ± 0.2 km s^{-1}) is also consistent with that measured by Riedel et al. (22.54 ± 1.16 km s^{-1}), all of which yield a very high membership probability ($P_{v+\pi} = 99.9\%$) in βPMG. The system also shows low-surface gravity based on

Table 6
Compilation of $v \sin i$ from the Literature

Name (2MASS)	Spectral Type	$v \sin i$ (km s^{-1})	$v \sin i$ (km s^{-1})
J01220441−3337036	K7Ve	4.9 ± 1.2[a]	<5.8[b]
J02365171−5203036	M2Ve	36.0 ± 3.6[a]	38.1 ± 3.5[b]
J02414683−5259523	K6Ve	80.4 ± 3.8[a]	80.0[c]
J02414730−5259306	M2.5V	10.4 ± 1.9[a]	8.0[c]
J04480066−5041255	K7Ve(vb)	5.4 ± 1.2[a]	<5.9[b]
J05332558−5117131	K7V	18.4 ± 1.2[a]	<6.2[b]
J11102788−3731520	M4Ve+M4Ve	11.6 ± 1.2[a]	<12.4[b]
J11211723−3446454	M1Ve	12.3 ± 1.2[a]	10.0[c]
J11211745−3446497	M1Ve	12.0 ± 1.2[a]	10.0[c]
J17130733−8552105	M0V	85.0[c]	99.2 ± 9.3[b]
J21100535−1919573	M2V	5.0[c]	9.7 ± 1.2[b]
J23261069−7323498	M0V(sb)	61.0 ± 0.8[a]	64.1 ± 8.6[b]
J23323085−1215513	M0Ve	8.8 ± 1.2[a]	<9.0[b]

Notes.
[a] Torres et al. 2006.
[b] This work.
[c] Glebocki & Gnacinski 2005.

the NaI8200 index. There is no lithium absorption which is expected for βPMG bona fide members near the lithium depletion boundary (Riedel et al. 2014; Yee & Jensen 2010) for βPMG. It is interesting to note that our analysis correctly predicts the binary nature of this star without knowledge of the parallax and the RV.

2MASSJ14252913−4113323 (SCR 1425-4113AB). This spectroscopic binary system (M2.5(sb)) was first proposed to be a potential member of TWA (with a marginal kinematic fit) by Riedel et al. (2014). Its NaI8200 index is consistent with a low-gravity object. It shows EW Li absorption (595 mÅ) consistent with a membership in TWA. However, our RV (-2.0 ± 1.6 km s^{-1}) is more consistent with a membership in βPMG with a predicted RV of -1.5 ± 1.8 km s^{-1} compared to 1.5 ± 2.8 km s^{-1} for TWA. When constrained with the trigonometric distance (66.9 ± 4.3 pc) measured by Riedel et al., our analysis yields a membership probability of 89.2% in βPMG assuming a binary system. This star is yet another system for which our analysis correctly predicts its binary nature without RV and parallax measurements. If in βPMG, this star would be the most distant M dwarf of the βPMG. However, given its relatively large distance combined with a large Li EW much more consistent with an association younger than βPMG (e.g., TWA), one should be cautious before assigning a bona fide membership to βPMG for SCR 1425-4113AB. This is beyond the scope of this paper but one should consider other distant associations (e.g., the Scorpius–Centaurus complex; Song et al. 2012) in our Bayesian analysis to firmly establish the membership of this young system. It is interesting to note that the star HIP 86598 (F9V) at 72 pc, formerly identified in βPMG by Kiss et al. (2011), was recently proposed by Song et al. (2012) to be a member of the Scorpius–Centaurus region.

6. DISCUSSION

Kinematics and Galactic positions alone are not sufficient to ascertain YMG membership, youth also needs to be established by verifying that candidates and bona fide members share similar measurements. Here we discuss how stellar rotation and X-ray luminosity can be used for constraining the age of young low-mass stars.

6.1. Rotation–Age Relation

Past studies of the rotation periods of stars in young clusters and in the field have established that stellar rotation is a function of mass, age, and magnetic activity, and that the rotation rates generally decrease with age (Soderblom 2010). The first parameterization of the empirical stellar rotation spin-down was introduced by Skumanich (1972), using projected rotational velocity as a proxy of the rotation rate. This parameterization takes the form of a power law, with an index of -0.5 ($v \sin i \, \alpha$ to $t^{-1/2}$). More recently, much attention has been paid to studying the stellar rotation rate evolution in the low-mass regime ($<1 \, M_{\odot}$), which eventually led to the development of gyrochronology (Barnes 2003, 2007).

One of the main outstanding problems within this area of research in understanding the angular momentum evolution of young late-type stars (K7V–M6V), for which the spin-up due to contraction competes with the spin-down due to magnetic braking (Reiners & Mohanty 2012). The stellar rotation rate evolution of M0V–M3V dwarfs can be broadly broken down into three main phases. During the first few million years, after the star is formed, the stellar rotation slows down due to interactions with the circumstellar disk. After the primordial disk dissipates, the stellar rotation rate increases until the star reaches the zero-age main sequence, and then finally decreases over time according to the power-law relation of Skumanich (1972). However, given the dispersion of rotation periods for old M dwarfs (Irwin et al. 2011), the exact exponent of the power law may depend on the magnetic field geometry of the stars. Observational data on the stellar rotation of low-mass stars at different ages and masses thus provide key insights into their evolution (Reiners & Mohanty 2012).

To help investigate how stellar rotation evolves as a function of age, we compiled measurements of $v \sin i$ for the M0V–M5V bona fide members of YMGs (see Table 9), which include seven stars from βPMG, four stars from ABDMG, and two stars for all THA, COL, CAR, and ARG YMGs. We excluded the binary systems from this analysis because their $v \sin i$ measurements could potentially be biased by blended line profiles, for spectroscopic binaries, and because stellar rotation evolution in binary systems could be affected by angular momentum exchanges between their components. We also compiled $v \sin i$ measurements for old M0V–M5V stars with a trigonometric parallax and X-ray detection from several sources (Delfosse et al. 1998; Glebocki & Gnacinski 2005; Reiners & Basri 2008; Jenkins et al. 2009; Lépine et al. 2013). This old sample comprises 39 stars and their properties are presented in Table 10.

Figure 5 (top) presents the cumulative distribution of $v \sin i$ for the M0V–M5V bona fide members of βPMG and ABDMG compared to that of the old sample. We estimated the median and dispersion of these distributions by fitting a lognormal function, as proposed by Weise et al. (2010). Table 11 summarizes the median $v \sin i$ along with their dispersion for YMG and field stars. As visible in Figure 5, there is a trend for $v \sin i$ to decrease with age between βPMG and field stars. We compared the distributions of $v \sin i$ pairwise by performing a double-sided Kolmogorov–Smirnov (K-S) test using the IDL routine *kstwo*. We found that field $v \sin i$ measurements are clearly not drawn from the same distribution as that of βPMG; the K-S probability that both distributions are the same is only 0.1%. The bottom panel of the Figure 5 presents the cumulative distributions of $v \sin i$ for our candidate members of the different YMGs with $P_v > 90\%$, along with the distribution for the old sample. Since

Table 7
Properties of Candidate Members of Young Kinematic Groups

Name (2MASS)	I_c[a] (mag)	J (mag)	$\mu_\alpha \cos\delta$[b] (mas yr^{-1})	μ_δ[b] (mas yr^{-1})	Spectral[c] Type	X-Ray[d] log(f_x)	Hα[e] (Å)	Li[f] (m Å)	$v \sin i$[g] (km s^{-1})	RV$_{meas}$[h] (km s^{-1})	RV$_{pred}$[i] (km s^{-1})	d_π[j] (pc)	d_s[i] (pc)	P[k] (%)	P_v[k] (%)	log L_x^s[d] (erg s^{-1})	Refs.
						β Pictoris moving group											
J00172353−6645124	9.94 ± 0.05	8.56 ± 0.02	104.3 ± 1.0	-13.5 ± 1.0	M2.5V	−11.77	6.0	···	<7.4[zz]	10.7 ± 0.2[zz]	10.9 ± 1.5	39.0 ± 2.6[vv]	35 ± 3	99.3	99.9	29.41 ± 0.19	18
J00275023−3233060	10.29 ± 0.03[vv]	8.88 ± 0.03	97.8 ± 1.1	-60.9 ± 4.0	M3.5Ve	−11.59	7.8	···	6.2 ± 1.8[zz]	8.8 ± 0.2[zz]	8.3 ± 1.4	32.3 ± 1.8[vv]	33 ± 2	1.8	99.9	29.53 ± 0.15	17
J00275035−3233238	10.48 ± 0.02[vv]	8.97 ± 0.03	117.4 ± 2.8	-29.3 ± 8.1	M3.5Ve	−11.59	5.3	···	<4.2[zz]	8.5 ± 0.2[zz]	8.3 ± 1.4	32.3 ± 1.8[vv]	32 ± 2	97.2	99.9	29.51 ± 0.15	17
J01132817−3821024	9.66 ± 0.07[o]	8.49 ± 0.02	123.0 ± 1.1	-38.3 ± 1.2	M0.0+M1.0	−11.77	2.5	···	<9.1[zz]	14.3 ± 0.5[zz]	11.9 ± 1.4	···	29 ± 2	16.7	99.3	···	18
J01365516−0647379	11.22 ± 0.06	9.71 ± 0.02	175.1 ± 4.4[y]	-98.8 ± 4.4[y]	M4V+>L0	−12.03	6.0	···	···	12.2 ± 0.4[uu]	9.5 ± 1.5	24.0 ± 0.4[uu]	21 ± 1	28.3	99.9	···	18

Notes.
[a] I_c magnitude from DENIS catalog (Epchtein et al. 1997), unless stated otherwise.
[b] Proper motion from UCAC3 catalog (Zacharias et al. 2009), unless stated otherwise.
[c] Spectral type with asterisk is for the whole unresolved system.
[d] *ROSAT* X-ray flux calculated from Riaz et al. (see Section 5.4; 2006) in erg s^{-1} cm^{-2}. L_x calculated from http://heasarc.gsfc.nasa.gov/W3Browse/all/rassdsstar.html.
[e] Hα EW from Riaz et al. (2006), unless stated otherwise.
[f] Lithium EW from Mentuch et al. (2008), unless stated otherwise.
[g] Projected rotational velocity from this work, unless stated otherwise.
[h] Radial velocity measurement from Montes et al. (2001), unless stated otherwise.
[i] Radial velocity and statistical distance derived by our analysis (see Malo et al. 2013; Section 5).
[j] Trigonometric distance from van Leeuwen (2007), unless stated otherwise.
[k] P: membership probability without considering the RV or parallax information; P_v: membership probability with considering the RV (see Malo et al. 2013; Section 5).
[l] Membership probability for which the binary hypothesis is higher.
(m) Torres et al. 2006; (n) van Leeuwen 2007; (o) Malo et al. 2013; (p) Magnitude without binary correction; Torres et al. 2006; Zuckerman et al. 2001c; (q) Reid et al. 2003; (r) Reid & Cruz 2002; (s) Koen et al. 2010; (t) Casagrande et al. 2008; (u) Reid et al. 2004; (v) UCAC4; Zacharias et al. 2013; (w) Moór et al. 2013; (x) Weinberger et al. 2013; (y) NOMAD; Zacharias et al. 2005; (z) PPMXL; Roeser et al. 2010; (aa) PPMX; Roeser et al. 2008; (bb) Looper et al. 2010; (cc) Binks & Jeffries 2014; (dd) Zickgraf et al. 2005; (ee) Shkolnik et al. 2011; (ff) Kiss et al. 2011; (gg) Herbig & Bell 1988; (hh) Shkolnik et al. 2009; (ii) da Silva et al. 2009; (jj) Kharchenko et al. 2007; (kk) RAVE; Zwitter et al. 2008; (ll) Gizis et al. 2002; (mm) See compilation in Table 5; (nn) See compilation in Table 6; (oo) Schlieder et al. 2010; (pp) Jayawardhana et al. 2006; (qq) Upgren & Harlow 1996; (rr) Hawley et al. 1996; (ss) Schlieder et al. 2012a; (tt) Bowler et al. 2013; (uu) Shkolnik et al. 2012; (vv) Riedel et al. 2014; (ww) Schlieder et al. 2012b; (xx) Rodriguez et al. 2011; (yy) Wahhaj et al. 2011; (zz) This work.
References. (1) Kastner et al. 1997; (2) Webb et al. 1999; (3) Torres et al. 2000; (4) Zuckerman et al. 2001b; (5) Zuckerman & Song 2004; (6) Torres et al. 2006; (7) Torres et al. 2008; (8) Lépine & Simon 2009; (9) Ortega et al. 2009; (10) Looper et al. 2010; (11) Schlieder et al. 2010; (12) Kiss et al. 2011; (13) Rodriguez et al. 2011; (14) Schlieder et al. 2012a ; (15) Bowler et al. 2013; (16) Shkolnik et al. 2012; (17) Riedel et al. 2014; (18) this work.

(This table is available in its entirety in a machine-readable form in the online journal. A portion is shown here for guidance regarding its form and content.)

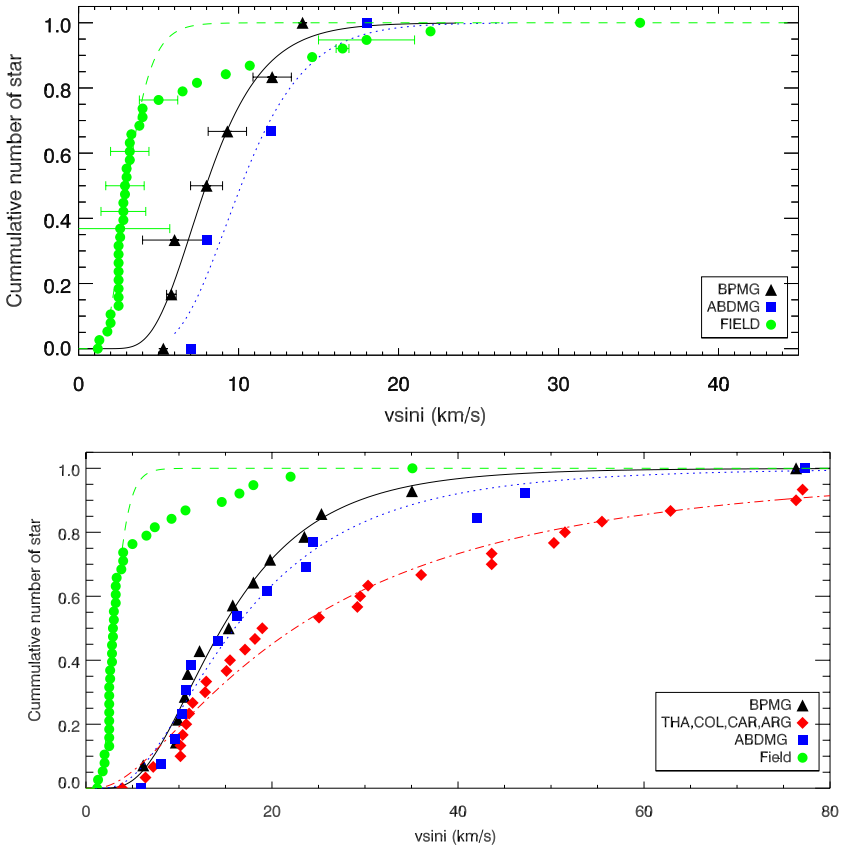

Figure 5. Top panel: $v \sin i$ cumulative distribution of M0V–M5V bona fide members excluding binaries (all kinds) compared to field distribution (filled green circles). The lines represent the adopted parameterization (see Table 11). Bottom panel: $v \sin i$ cumulative distribution of candidate members excluding binary systems.
(A color version of this figure is available in the online journal.)

Table 8
Membership Probabilities of All Candidates[a]

Name	βPMG			TWA			THA			COL			CAR			ARG			ABDMG			Field		
	P	P_v	$P_{v+\pi}$	P	P_v	$P_{v+\pi}$	P	P_v	$P_{v+\pi}$	P	P_v	$P_{v+\pi}$	P	P_v	$P_{v+\pi}$	P	P_v	$P_{v+\pi}$	P	P_v	$P_{v+\pi}$	P	P_v	$P_{v+\pi}$
J00172353−6645124	99.3	99.9	99.9	0.0	0.0	0.0	0.0	0.0	0.0	0.0	0.0	0.0	0.0	0.0	0.0	0.5	0.0	0.0	0.1	0.0	0.0	0.0	0.0	0.0
J00275023−3233060	1.8	99.9	99.9	0.0	0.0	0.0	94.6[b]	0.0	0.0	3.6[b]	0.0	0.0	0.0	0.0	0.0	0.0	0.0	0.0	0.1	0.2	0.0	0.0	0.2	0.0
J00275035−3233238	97.2	99.9	99.9	0.0	0.0	0.0	2.2[b]	0.0	0.0	0.3	0.0	0.0	0.0	0.0	0.0	0.1	0.0	0.0	0.0	0.0	0.0	0.1	0.0	0.0
J00281434−3227556	81.1	83.6	···	0.0	0.0	···	16.4[b]	12.0[b]	···	2.4[b]	4.4[b]	···	0.0	0.0	···	0.0	0.0	···	0.0	0.0	···	0.1	0.1	···
J00340843+2523498	0.0	0.0	···	0.0	0.0	···	0.0	0.0	···	0.0	0.0	···	0.0	0.0	···	0.0	0.0	···	99.4	99.9	···	0.6	0.1	···

Notes.
[a] Membership probability (P), membership probability including radial velocity information (P_v), or membership probability including radial velocity and parallax information ($P_{v+\pi}$).
[b] Membership probability (P or P_v or $P_{v+\pi}$) for which the binary hypothesis has a higher probability.
(This table is available in its entirety in a machine-readable form in the online journal. A portion is shown here for guidance regarding its form and content.)

our detection limits are between 3 and 8 km s^{-1}, depending on the slowly rotating standard stars used, we reached only upper limits on $v \sin i$ for 28 candidates (see Table 7); these candidates were excluded from the figure.

To quantify the similarity between our samples of candidates and the bona fide members, we once again performed a K-S test as above. Overall the candidate distributions are very similar to the bona fide YMG distributions with K-S probabilities of 20%–73%. Accordingly, the probabilities that the $v \sin i$ of our candidates were drawn from the same distribution as those of the field sample are very low, 0.0002%–0.0003%. Similar results were also found by Scholz et al. (2007). It thus appears empirically that young low-mass stars in the age range defined by βPMG and ABDMG have larger $v \sin i$ than their old counterparts in the field. In our candidates sample, there are 22 ultrafast rotators (>50 km s^{-1}), including 8 stars that were identified as binary systems; for the 14 remaining fast rotators we cannot rule out the possibility that they are also unresolved binary systems.

6.2. X-Ray Luminosity–Age Relation

Past studies on stellar activity of low-mass stars have shown a saturation limit when the $v \sin i$ is compared to the R_X parameter, the ratio of X-ray to bolometric luminosity (Preibisch & Feigelson 2005; Mamajek & Hillenbrand 2008). This parameter is convenient as an activity proxy because it is

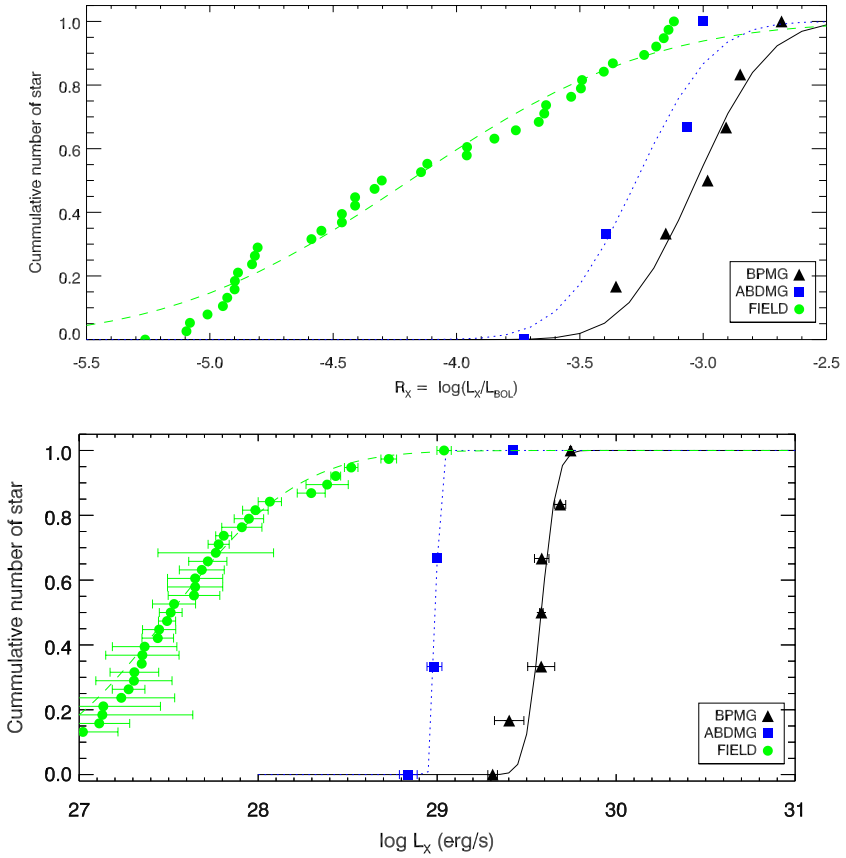

Figure 6. Top panel: cumulative distribution of R_X ($\log L_X/L_{bol}$) for M0V–M5V bona fide members, which exclude binaries. Bottom panel: $\log L_X$ cumulative distribution for M0V–M5V bona fide members of βPMG (black triangles), and ABDMG (blue squares).
(A color version of this figure is available in the online journal.)

Table 9
Properties of Bona Fide Members

Name of Star	$v \sin i$ [a] (km s^{-1})	π [b] (mas)	R_x	$\log L_x$ (erg s^{-1})
		βPMG		
HIP 11152	6.0 ± 2.0[c]	34.86 ± 2.84	−2.85	29.58 ± 0.08
HIP 23200	14.0	38.64 ± 2.54	−3.15	29.58 ± 0.01
HIP 23309	5.8 ± 0.3	37.34 ± 1.13	−3.37	29.40 ± 0.08
HIP 50156	8.0 ± 1.0[d]	43.32 ± 1.80	−3.35	29.31 ± 0.03
HIP 102409	9.3 ± 1.2	100.91 ± 1.06	−2.98	29.75 ± 0.01
HIP 112312	12.1 ± 1.2	42.84 ± 3.61	−2.68	29.69 ± 0.03
GJ 3331 A	5.3[e]	51.98 ± 1.30[f]	−2.91	29.58 ± 0.04
		ABDMG		
HIP 17695	18.0[g]	62.00 ± 2.88	−3.07	29.00 ± 0.02
HIP 31878	12.0[g]	44.74 ± 0.91	−3.70	28.84 ± 0.05
HIP 81084	7.0[g]	32.60 ± 2.47	−3.40	28.98 ± 0.04
HIP 114066	8.0[g]	40.81 ± 1.60	−3.00	29.42 ± 0.01

Notes.
[a] Projected rotation velocity measurement from Torres et al. (2006), unless stated otherwise.
[b] Parallax measurement from van Leeuwen (2007), unless stated otherwise.
[c] Schlieder et al. (2010).
[d] Herrero et al. (2012).
[e] Reiners et al. (2012).
[f] Riedel et al. (2014).
[g] da Silva et al. (2009).

independent of distance but it must rely on an estimate of the bolometric flux of the star. In order to quantify the sensitivity of the R_X parameter versus age for YMG stars, we have compiled *ROSAT* X-ray luminosities of all known bona fide low-mass members with spectral type later than M0V. This sample comprises 13 M stars. The bolometric luminosities are determined using the *J*-band bolometric correction presented in Pecaut & Mamajek (2013, see their Table 6, using $J-H$ index) for βPMG members and the *J*-band bolometric correction from Casagrande et al. (2008, see their Equation (5)) for ABDMG members and field dwarfs. Again, all binary systems were excluded.

The upper panel of Figure 6 presents the cumulative distribution of R_X for young bona fide members and old field dwarfs. While one can see a clear difference between young and old stars, there is no obvious distinction between βPMG and ABDMG members.

The bottom panel of Figure 6 presents the cumulative distribution of $\log L_X$ for M0V–M5V bona fide members compared to the old low-mass population. The X-ray luminosity is calculated using this formulae[9]: $L_x = 1.2e^{38} f_x d_\pi^2$. One clearly see a difference of ∼0.6 dex between βPMG and ABDMG members. Even if we take into account the uncertainties on the *ROSAT* counts, HR1 ratio and parallax (error bar on Figure 6), the difference between the two young samples is significant. A K-S test performed on both distributions shows that they are different at a confidence level of 94.4%. We estimated the mean and dispersion of each distribution by fitting error functions (see Table 11).

[9] http://heasarc.gsfc.nasa.gov/W3Browse/all/rassdsstar.html

Table 10
Compilation of X-Ray Emission from Field M Dwarfs

Name (2MASS)	Spectral Type	$\log f_X$[a] (erg s^{-1} cm^{-2})	π (mas)	$\log L_X$[a] (erg s^{-1})	R_X	$v \sin i$ (km s^{-1})
J01123052−1659570	M4.5V	−11.73 ± 0.07	269.10 ± 7.60[c]	27.49 ± 0.05	−3.54	2.50[i]
J02001278+1303112	M4.5V	−11.94 ± 0.11	222.00 ± 5.00[d]	27.45 ± 0.09	−3.64	3.80[j]
J02164119−3059181	M3V	−11.87 ± 0.08	69.81 ± 3.10[c]	28.52 ± 0.04	−3.37	5.00[k]
J02441537+2531249	M3V	−12.52 ± 0.23	133.16 ± 2.26[c]	27.31 ± 0.21	−4.55	2.80[g]
J05015746−0656459	M4V	−12.31 ± 0.14	163.00 ± 26.00[e]	27.35 ± 0.00	−3.96	3.20[e]
J06000351+0242236	M4V	−11.53 ± 0.08	190.90 ± 1.90[f]	27.98 ± 0.07	−3.49	7.40[g]
J10112218+4927153	M0V	−12.02 ± 0.09	205.21 ± 0.54[c]	27.44 ± 0.09	−5.26	2.80[j]
J10121768−0344441	M1.5V	−12.51 ± 0.19	127.08 ± 1.90[c]	27.37 ± 0.18	−4.90	1.80[i]
J11474440+0048164	M4V	−12.28 ± 0.16	300.00 ± 1.50[g]	26.84 ± 0.16	−4.41	2.00[g]
J11510737+3516188	M1V	−12.30 ± 0.16	116.48 ± 1.19[c]	27.65 ± 0.15	−4.46	3.30[g]
J11314655−4102473	M3.5V	−11.38 ± 0.07	96.56 ± 2.39[c]	28.73 ± 0.04	−3.14	18.00[j]
J13295979+1022376	M0.5V	−12.44 ± 0.22	138.70 ± 2.90[g]	27.35 ± 0.20	−4.83	1.30[g]
J17283991−4653424	M3V	−11.86 ± 0.13	220.24 ± 1.42[c]	27.53 ± 0.12	−4.33	3.20[k]
J18073292−1557464	M4.5V	−11.90 ± 0.11	130.00 ± 3.70[g]	27.95 ± 0.08	−3.12	3.00[i]
J18185725+6611332	M4.5V	−12.49 ± 0.04	137.50 ± 27.50[h]	27.31 ± 0.14	−3.67	14.60[i]
J18494929−2350101	M3.5V	−11.25 ± 0.06	336.72 ± 2.03[c]	27.78 ± 0.06	−3.50	4.00[i]
J19510930+4628598	M4V	−12.16 ± 0.09	84.10 ± 2.40[h]	28.06 ± 0.06	−3.40	22.00[i]
J20303207+6526586	M2.5V	−12.11 ± 0.07	120.00 ± 3.10[g]	27.81 ± 0.04	−4.14	3.20[g]
J20531977+6209156	M0.5V	−12.34 ± 0.09	130.00 ± 3.60[g]	27.51 ± 0.06	−4.93	2.80[g]
J22011310+2818248	M4V	−11.55 ± 0.05	112.30 ± 3.00[c]	28.43 ± 0.03	−3.19	35.10[i]
J23415498+4410407	M5V	−11.79 ± 0.09	320.00 ± 1.10[g]	27.28 ± 0.09	−3.76	1.20[g]
J23430628+3632132	M4V	−12.20 ± 0.13	120.00 ± 2.90[g]	27.72 ± 0.11	−3.64	2.60[g]
J23491255+0224037	M1V	−12.47 ± 0.20	177.90 ± 5.60[g]	27.11 ± 0.17	−4.89	3.00[g]
J04374092+5253372	M0.5V	−12.40 ± 0.13	98.91 ± 1.01[c]	27.68 ± 0.13	−4.81	2.60[j]
J05420897+1229252	M4V	−13.08 ± 0.39	171.60 ± 4.00[c]	26.53 ± 0.36	−4.95	2.90[g]
J09411033+1312344	M1.5V	−12.39 ± 0.20	88.81 ± 1.68[c]	27.79 ± 0.19	−4.32	2.50[i]
J09535523+2056460	M4.5V	−12.87 ± 0.34	108.40 ± 2.30[g]	27.13 ± 0.32	−3.85	16.50[g]
J09560868+6247185	M0V	−12.49 ± 0.16	94.68 ± 1.26[c]	27.64 ± 0.14	−4.82	2.50[i]
J10251088−1013434	M1V	−13.13 ± 0.53	81.00 ± 1.91[c]	27.13 ± 0.51	−5.09	2.50[i]
J11023832+2158017	M0V	−11.84 ± 0.13	84.95 ± 1.05[c]	28.39 ± 0.12	−3.96	2.50[i]
J11474440+0048164	M4V	−12.28 ± 0.16	298.04 ± 2.30[c]	26.85 ± 0.15	−4.41	2.00[g]
J11510737+3516188	M1V	−12.30 ± 0.16	116.48 ± 1.19[c]	27.65 ± 0.15	−4.46	2.50[i]
J12375231−5200055	M3V	−12.14 ± 0.13	103.18 ± 2.31[c]	27.91 ± 0.11	−4.12	2.90[k]
J14021961+1341229	M0.5V	−12.91 ± 0.36	50.36 ± 2.04[c]	27.76 ± 0.32	−4.59	4.00[i]
J15215291+2058394	M1.5V	−11.16 ± 0.06	87.63 ± 1.81[c]	29.04 ± 0.04	−3.24	6.50[i]
J16252459+5418148	M2V	−13.00 ± 0.29	153.46 ± 0.99[c]	26.71 ± 0.28	−5.08	2.50[i]
J16570570−0420559	M3.5V	−11.66 ± 0.09	115.40 ± 1.50[f]	28.30 ± 0.08	−3.16	10.70[i]
J17435595+4322441	M2.5V	−13.01 ± 0.21	105.50 ± 1.18[c]	27.02 ± 0.20	−5.01	2.50[i]
J18050755−0301523	M1.0V	−12.62 ± 0.31	128.89 ± 1.43[c]	27.24 ± 0.30	−4.90	2.50[i]

Notes.
[a] *ROSAT* X-ray flux calculated from Riaz et al. (2006, Section 5.4) in erg s^{-1} cm^{-2}.
[b] *ROSAT* X-ray luminosity calculated from formulae on http://heasarc.gsfc.nasa.gov/W3Browse/all/rassdsstar.html.
[c] van Leeuwen (2007).
[d] Houdebine (2012).
[e] Delfosse et al. (1998).
[f] Lépine & Gaidos (2011).
[g] Jenkins et al. (2009).
[h] Lepine & Shara (2005).
[i] Reiners et al. (2012).
[j] Glebocki & Gnacinski (2005).
[k] Torres et al. (2006).

We note that Preibisch & Feigelson (2005) found similar results for Chamaeleon association and the Pleiades group, where these two groups have similar ages compared to βPMG and ABDMG. Overall, relatively young stars represented by βPMG members are two orders of magnitude more luminous than M dwarfs in the field and this luminosity excess remains significant (a factor of ∼4) compared to older AMDMG members. This analysis shows that the X-ray luminosity is an excellent youth indicator for M dwarfs in the age range defined by βPMG and ABDMG members. This youth diagnostic is very complementary to the common method of using the presence of the lithium resonance line at 6707.8 Å. However, since lithium is rapidly depleted in M dwarfs, especially fully convective ones (∼M3V), lithium is a useful youth indicator only for low-mass stars younger than a few 10^7 yr. Using the X-ray luminosity as youth indicator extends by roughly an order of magnitude the age range covered by the lithium method.

We performed the same analysis on our candidate members, where the X-ray luminosity was determined using the statistical distance (see Table 7), as a proxy of the parallax ($\log L_X^s$). As

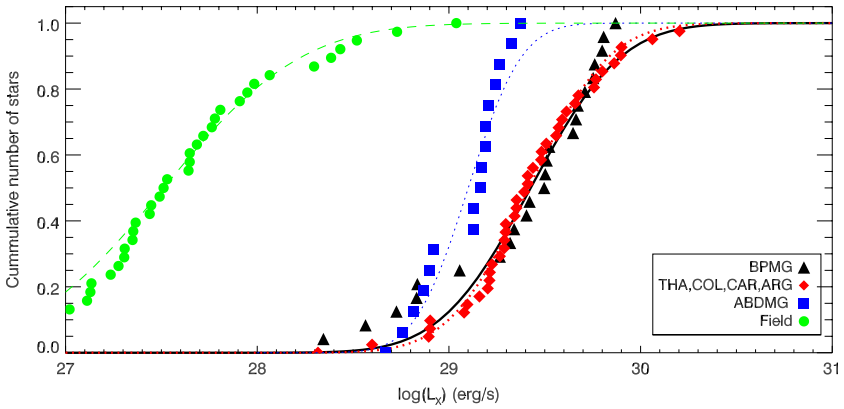

Figure 7. Cumulative distribution of log L_X^s for candidate members excluding binary systems compared to old field log L_X distribution.
(A color version of this figure is available in the online journal.)

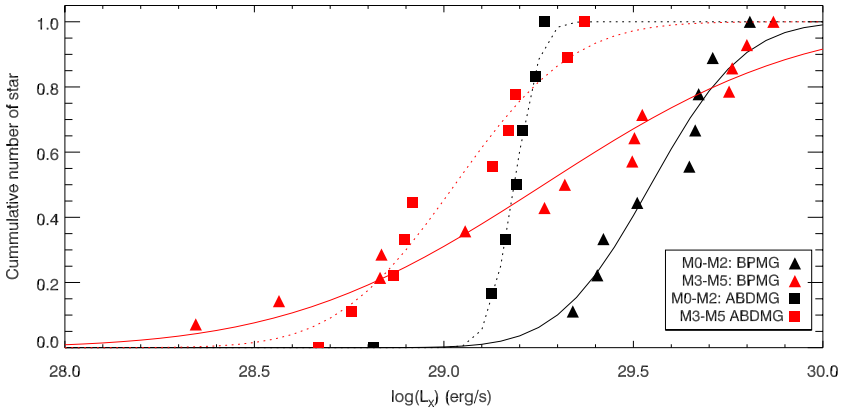

Figure 8. Cumulative distribution of log L_X for M0V–M2V and M3V–M5V of βPMG and ABDMG candidate members.
(A color version of this figure is available in the online journal.)

Table 11
log L_X and $v \sin i$ Average Properties

Group of Stars	log L_X (erg s^{-1})	$\sigma_{\log L_X}$ (erg s^{-1})	$v \sin i$ (km s^{-1})	$\sigma_{v \sin i}$ (km s^{-1})	Number[a] of Stars
		βPMG			
M0–M5 Bona fide	29.6	0.1	8.0	1.4	7, 7
M0–M5 Candidate	29.4	0.4	14.6	1.7	25, 15
M0–M2 Candidate	29.5	0.2	...	...	10
M3–M5 Candidate	29.3	0.5	...	...	15
		THA, COL, CAR, and ARG			
M0–M5 Bona fide	...	...	...	...	2
M0–M5 Candidate	29.4	0.3	22.5	2.5	42, 31
		ABDMG			
M0–M5 Bona fide	29.0	0.1	10.0	1.4	4, 4
M0–M5 Candidate	29.1	0.2	16.0	1.9	17, 14
M0–M2 Candidate	29.2	0.1	...	...	7
M3–M5 Candidate	29.0	0.2	...	...	10
		Field			
M0–M5	27.5	0.6	3.1	1.4	39, 39

Note. [a] Number of stars with L_x and $v \sin i$ measurements, respectively.

shown in Paper I, the statistical distance is a reliable estimate of the true distance within an uncertainty of ~10%. Figure 7 presents the cumulative distribution of log L_X^s for our highly probable members compared to the low-mass field dwarfs. The amplitude of the error bars is ~0.3 dex and take into account the uncertainties on both the *ROSAT* flux and the statistical distance. The same trend for the X-ray luminosity to increase at young ages is confirmed with the candidates. One can see in Figure 7

that the βPMG distribution shows an excess of low-luminosity objects which could find an explanation if the statistical distance of these objects is somewhat different from reality. In fact, we do have a parallax for one βPMG candidate member and indeed, when one uses the true distance to infer its X-ray luminosity, its value is brought much closer to the nominal distribution for this association.

In order to investigate the behavior of the X-ray luminosity with spectral type (mass), we divide our candidates into two groups: M0V–M2V (partly convective stars) and M3V–M5V (fully convective stars). Figure 8 presents the cumulative distribution of X-ray luminosity, for both groups in βPMG and ABDMG. Table 11 summarizes the median $\log L_X$ along with their dispersion for YMGs and field stars. The X-ray luminosity for M3V–M5V βPMG candidates is slightly lower (with a higher dispersion) compared to the M0V–M2V group, and the same behavior is seen for ABDMG candidate members. More observations are clearly needed to confirm this trend which may provide some insights for understanding the X-ray property and magnetic activity of low-mass stars near the brown dwarf boundary.

7. SUMMARY AND CONCLUSION

The study aims at extending the census of low-mass star members of seven young nearby associations. A Bayesian statistical analysis described in Paper I was developed for identifying candidates based on a minimal set of observables (proper motion, photometry, position in the sky) combined with a kinematic model of the association. This method yields a membership probability to a given association as well as the most probable (statistical) distance and the predicted RV. In the present study, RV measurements were used to better constrain the membership of the candidates.

Starting from a sample of 920 stars, all showing indicators of youth such as Hα and/or X-ray emission, our analysis selected 247 candidates with a membership probability over 90%. To confirm the predicted membership, we have secured RV measurements for 202 candidate members. These measurements were combined with a compilation of 166 measurements from the literature to select a list of 130 young K and M stars with a membership probability to all YMGs exceeding 90% when the RV is included in our Bayesian analysis. A subgroup of 117 candidates are associated with a single YMG distributed as follows: 27 in βPMG, 22 in THA, 25 in COL, 7 in CAR, 18 in ARG, and 18 in ABDMG.

We investigated the rotation–age relation and found that stellar rotation ($v \sin i$) of young M dwarfs is significantly higher compared the their field counterparts. We also find that the X-ray luminosity of ~12–22 Myr old βPMG members are typically two orders of magnitude more luminous compared to field stars; this luminosity excess is a factor of ~4 compared to older (~100 Myr) ABDMG members. Thus, the X-ray luminosity appears to be an excellent age discriminant for M dwarfs.

This work has unveiled a large population of highly probable low-mass members to nearby YMGs. A parallax, and ideally other indications of youth, are mandatory to firmly establish them as bona fide members of their respective association.

The authors thank Bernadette Rogers, German Gimeno, Michele Edwards, Elena Valenti, and the Gemini, CFHT, and ESO staff for carrying out the observations. Special thanks to Anne-Marie Lagrange, Ansgar Reiners, and Evgenya Shkolnik for interesting advices. Finally, we thank our referee for several comments which improved the quality of this paper.

This work was supported in part through grants from the Fond de Recherche Québécois—Nature et Technologie and the Natural Science and Engineering Research Council of Canada. This research has made use of the SIMBAD database, operated at Centre de Données astronomiques de Strasbourg (CDS), Strasbourg, France. This research has made use of the VizieR catalogue access tool, CDS, Strasbourg, France (Ochsenbein et al. 2000).

Based on observations obtained at the Gemini Observatory, which is operated by the Association of Universities for Research in Astronomy, Inc., under a cooperative agreement with the NSF on behalf of the Gemini partnership: the National Science Foundation (United States), the Science and Technology Facilities Council (United Kingdom), the National Research Council (Canada), CONICYT (Chile), the Australian Research Council (Australia), Ministério da Ciência, Tecnologia e Inovação (Brazil), and Ministerio de Ciencia, Tecnología e Innovación Productiva (Argentina).

The DENIS project has been partly funded by the SCIENCE and the HCM plans of the European Commission under grants CT920791 and CT940627. It is supported by INSU, MEN, and CNRS in France, by the State of Baden-Württemberg in Germany, by DGICYT in Spain, by CNR in Italy, by FFwFBWF in Austria, by FAPESP in Brazil, by OTKA grants F-4239 and F-013990 in Hungary, and by the ESO C&EE grant A-04-046. Jean Claude Renault from IAP was the Project manager. Observations were carried out, thanks to the contribution of numerous students and young scientists from all involved institutes, under the supervision of P. Fouqué, survey astronomer resident in Chile.

Funding for RAVE has been provided by the Australian Astronomical Observatory; the Leibniz-Institut fuer Astrophysik Potsdam (AIP); the Australian National University; the Australian Research Council; the French National Research Agency; the German Research Foundation (SPP 1177 and SFB 881); the European Research Council (ERC-StG 240271 Galactica); the Istituto Nazionale di Astrofisica at Padova; the Johns Hopkins University; the National Science Foundation of the USA (AST-0908326); the W. M. Keck foundation; the Macquarie University; the Netherlands Research School for Astronomy; the Natural Sciences and Engineering Research Council of Canada; the Slovenian Research Agency; the Swiss National Science Foundation; the Science & Technology Facilities Council of the UK; Opticon; Strasbourg Observatory; and the Universities of Groningen, Heidelberg and Sydney. The RAVE Web site is at http://www.rave-survey.org.

REFERENCES

Anderson, E., & Francis, C. 2012, AstL, 38, 331
Barnes, S. A. 2003, ApJ, 586, 464
Barnes, S. A. 2007, ApJ, 669, 1167
Barrado Y Navascués, D. 2006, A&A, 459, 511
Barrado y Navascués, D., Stauffer, J. R., & Jayawardhana, R. 2004, ApJ, 614, 386
Bergfors, C., Brandner, W., Janson, M., et al. 2010, A&A, 520, A54
Binks, A. S., & Jeffries, R. D. 2014, MNRAS, 438, L11
Bobylev, V. V., & Bajkova, A. T. 2007, AstL, 33, 571
Bobylev, V. V., Goncharov, G. A., & Bajkova, A. T. 2007, yCat, 908, 30821
Bowler, B. P., Liu, M. C., Shkolnik, E. L., & Dupuy, T. J. 2013, ApJ, 774, 55
Bowler, B. P., Liu, M. C., Shkolnik, E. L., & Tamura, M. 2012, ApJ, 756, 69
Casagrande, L., Flynn, C., & Bessell, M. 2008, MNRAS, 389, 585
Chubak, C., Marcy, G., Fischer, D. A., et al. 2012, arXiv:1207.6212
da Silva, L., Torres, C. A. O., de La Reza, R., et al. 2009, A&A, 508, 833
Daemgen, S., Siegler, N., Reid, I. N., & Close, L. M. 2007, ApJ, 654, 558

de Bruijne, J. H. J., & Eilers, A.-C. 2012, A&A, 546, A61
de la Reza, R., Torres, C. A. O., Quast, G., Castilho, B. V., & Vieira, G. L. 1989, ApJL, 343, L61
Delfosse, X., Beuzit, J.-L., Marchal, L., et al. 2004, in ASP Conf. Ser. 318, Spectroscopically and Spatially Resolving the Components of the Close Binary Stars, ed. R. W. Hilditch, H. Hensberge, & K. Pavlovski (San Francisco, CA: ASP), 166
Delfosse, X., Forveille, T., Perrier, C., & Mayor, M. 1998, A&A, 331, 581
Donati, J.-F., Catala, C., Landstreet, J. D., & Petit, P. 2006, in ASP Conf. Ser. 358, Solar Polarization 4, ed. R. Casini & B. W. Lites (San Francisco, CA: ASP), 362
Donati, J.-F., Semel, M., Carter, B. D., Rees, D. E., & Collier Cameron, A. 1997, MNRAS, 291, 658
Epchtein, N., de Batz, B., Capoani, L., et al. 1997, Msngr, 87, 27
Gagné, J., Lafrenière, D., Doyon, R., et al. 2013, MmSAI, 84, 916
Gálvez-Ortiz, M. C., Clarke, J. R. A., Pinfield, D. J., et al. 2010, MNRAS, 409, 552
Gizis, J. E., Reid, I. N., & Hawley, S. L. 2002, AJ, 123, 3356
Glebocki, R., & Gnacinski, P. 2005, yCat, 3244, 0
Gray, D. F. 1992, The Observation and Analysis of Stellar Photospheres (Cambridge: Cambridge Univ. Press)
Hawley, S. L., Gizis, J. E., & Reid, I. N. 1996, AJ, 112, 2799
Herbig, G. H., & Bell, K. R. 1988, Third Catalog of Emission-Line Stars of the Orion Population (Santa Cruz, CA: Lick Observatory), 3
Herrero, E., Ribas, I., Jordi, C., Guinan, E. F., & Engle, S. G. 2012, A&A, 537, A147
Hinkle, K. H., Blum, R. D., Joyce, R. R., et al. 2003, Proc. SPIE, 4834, 353
Houdebine, E. R. 2012, MNRAS, 421, 3189
Irwin, J., Berta, Z. K., Burke, C. J., et al. 2011, ApJ, 727, 56
Janson, M., et al. 2012, ApJ, 754, 44
Jayawardhana, R., Coffey, J., Scholz, A., Brandeker, A., & van Kerkwijk, M. H. 2006, ApJ, 648, 1206
Jenkins, J. S., Ramsey, L. W., Jones, H. R. A., et al. 2009, ApJ, 704, 975
Kaeufl, H.-U., Ballester, P., Biereichel, P., et al. 2004, Proc. SPIE, 5492, 1218
Kastner, J. H., Zuckerman, B., Weintraub, D. A., & Forveille, T. 1997, Sci, 277, 67
Kharchenko, N. V., Scholz, R., Piskunov, A. E., Roeser, S., & Schilbach, E. 2007, yCat, 3254, 0
Kiss, L. L., Moór, A., Szalai, T., et al. 2011, MNRAS, 411, 117
Koen, C., Kilkenny, D., van Wyk, F., & Marang, F. 2010, MNRAS, 403, 1949
Landolt, A. U. 2009, AJ, 137, 4186
Leinert, C., Henry, T., Glindemann, A., & McCarthy, D. W., Jr. 1997, A&A, 325, 159
Lépine, S., & Gaidos, E. 2011, AJ, 142, 138
Lépine, S., Hilton, E. J., Mann, A. W., et al. 2013, AJ, 145, 102
Lepine, S., & Shara, M. M. 2005, yCat, 1298, 0
Lépine, S., & Simon, M. 2009, AJ, 137, 3632
Liu, M. C., Dupuy, T. J., & Allers, K. N. 2013, AN, 334, 85
Looper, D. L., Bochanski, J. J., Burgasser, A. J., et al. 2010, AJ, 140, 1486
López-Santiago, J., Micela, G., & Montes, D. 2009, A&A, 499, 129
López-Santiago, J., Montes, D., Crespo-Chacón, I., & Fernández-Figueroa, M. J. 2006, ApJ, 643, 1160
López-Santiago, J., Montes, D., Gálvez-Ortiz, M. C., et al. 2010, A&A, 514, A97
Luhman, K. L., Stauffer, J. R., & Mamajek, E. E. 2005, ApJL, 628, L69
Lyo, A.-R., Lawson, W. A., & Bessell, M. S. 2004, MNRAS, 355, 363
Makarov, V. V. 2007, ApJS, 169, 105
Makarov, V. V., & Urban, S. 2000, MNRAS, 317, 289
Malo, L., Doyon, R., Lafrenière, D., et al. 2013, ApJ, 762, 88
Mamajek, E. E., & Hillenbrand, L. A. 2008, ApJ, 687, 1264
Mazeh, T., Prato, L., Simon, M., et al. 2002, ApJ, 564, 1007
Mentuch, E., Brandeker, A., van Kerkwijk, M. H., Jayawardhana, R., & Hauschildt, P. H. 2008, ApJ, 689, 1127
Messina, S., Desidera, S., Turatto, M., Lanzafame, A. C., & Guinan, E. F. 2010, A&A, 520, A15
Montes, D., López-Santiago, J., Gálvez, M. C., et al. 2001, MNRAS, 328, 45
Moór, A., Szabó, G. M., Kiss, L. L., et al. 2013, MNRAS, 435, 1376
Nidever, D. L., Marcy, G. W., Butler, R. P., Fischer, D. A., & Vogt, S. S. 2002, ApJS, 141, 503
Ochsenbein, F., Bauer, P., & Marcout, J. 2000, A&AS, 143, 23
Ortega, V. G., Jilinski, E., de la Reza, R., & Bazzanella, B. 2009, AJ, 137, 3922
Pecaut, M. J., & Mamajek, E. E. 2013, ApJS, 208, 9
Preibisch, T., & Feigelson, E. D. 2005, ApJS, 160, 390
Reid, I. N., & Cruz, K. L. 2002, AJ, 123, 2806
Reid, I. N., Cruz, K. L., Allen, P., et al. 2003, AJ, 126, 3007
Reid, I. N., Cruz, K. L., Allen, P., et al. 2004, AJ, 128, 463
Reiners, A., & Basri, G. 2008, ApJ, 684, 1390
Reiners, A., Joshi, N., & Goldman, B. 2012, AJ, 143, 93
Reiners, A., & Mohanty, S. 2012, ApJ, 746, 43
Riaz, B., Gizis, J. E., & Harvin, J. 2006, AJ, 132, 866
Riedel, A. R., Murphy, S. J., Henry, T. J., et al. 2011, AJ, 142, 104
Riedel, A. R., Subasavage, J. P., Finch, C. T., et al. 2010, AJ, 140, 897
Riedel, A. R., et al. 2014, AJ, 147, 85
Rodriguez, D. R., Bessell, M. S., Zuckerman, B., & Kastner, J. H. 2011, ApJ, 727, 62
Rodriguez, D. R., Zuckerman, B., Kastner, J. H., et al. 2013, ApJ, 774, 101
Roeser, S., Demleitner, M., & Schilbach, E. 2010, AJ, 139, 2440
Roeser, S., Schilbach, E., Schwan, H., et al. 2008, yCat, 1312, 0
Rousselot, P., Lidman, C., Cuby, J.-G., Moreels, G., & Monnet, G. 2000, A&A, 354, 1134
Schlieder, J. E., Lépine, S., & Simon, M. 2010, AJ, 140, 119
Schlieder, J. E., Lépine, S., & Simon, M. 2012a, AJ, 143, 80
Schlieder, J. E., Lepine, S., & Simon, M. 2012b, AJ, 144, 109
Scholz, A., Coffey, J., Brandeker, A., & Jayawardhana, R. 2007, ApJ, 662, 1254
Shkolnik, E., Liu, M. C., & Reid, I. N. 2009, ApJ, 699, 649
Shkolnik, E. L., Anglada-Escude, G., Liu, M. C., et al. 2012, ApJ, 758, 56
Shkolnik, E. L., Hebb, L., Liu, M. C., Reid, I. N., & Cameron, A. C. 2010, ApJ, 716, 1522
Shkolnik, E. L., Liu, M. C., Reid, I. N., Dupuy, T., & Weinberger, A. J. 2011, ApJ, 727, 6
Skiff, B. A. 2010, yCat, 1, 2023
Skrutskie, M. F., Cutri, R. M., Stiening, R., et al. 2006, AJ, 131, 1163
Skumanich, A. 1972, ApJ, 171, 565
Slesnick, C. L., Carpenter, J. M., & Hillenbrand, L. A. 2006, AJ, 131, 3016
Soderblom, D. R. 2010, ARA&A, 48, 581
Song, I., Zuckerman, B., & Bessell, M. 2012, AJ, 144, 8
Song, I., Zuckerman, B., & Bessell, M. S. 2003, ApJ, 599, 342
Soubiran, C., Jasniewicz, G., Chemin, L., et al. 2013, A&A, 552, A64
Steinmetz, M., Zwitter, T., Siebert, A., et al. 2006, AJ, 132, 1645
Torres, C. A. O., da Silva, L., Quast, G. R., de la Reza, R., & Jilinski, E. 2000, AJ, 120, 1410
Torres, C. A. O., Quast, G. R., da Silva, L., et al. 2006, A&A, 460, 695
Torres, C. A. O., Quast, G. R., de La Reza, R., da Silva, L., & Melo, C. H. F. 2001, in ASP Conf. Ser. 244, Young Stars Near Earth: Progress and Prospects, ed. R. Jayawardhana & T. Greene (San Francisco, CA: ASP), 43
Torres, C. A. O., Quast, G. R., Melo, C. H. F., & Sterzik, M. F. 2008, in Handbook of Star-forming Regions Volume II: The Southern Sky, ed. B. Reipurth (San Francisco, CA: ASP), 757
Upgren, A. R., & Harlow, J. J. B. 1996, PASP, 108, 64
van Leeuwen, F. 2007, A&A, 474, 653
Wahhaj, Z., Liu, M. C., Biller, B. A., et al. 2011, ApJ, 729, 139
Webb, R. A., Zuckerman, B., Platais, I., et al. 1999, ApJL, 512, L63
Weinberger, A. J., Anglada-Escudé, G., & Boss, A. P. 2013, ApJ, 762, 118
Weise, P., Launhardt, R., Setiawan, J., & Henning, T. 2010, A&A, 517, A88
Wright, E. L., Eisenhardt, P. R. M., Mainzer, A. K., et al. 2010, AJ, 140, 1868
Yee, J. C., & Jensen, E. L. N. 2010, ApJ, 711, 303
York, D. G., Adelman, J., Anderson, J. E., Jr., et al. 2000, AJ, 120, 1579
Zacharias, N., Finch, C., Girard, T., et al. 2009, yCat, 1315, 0
Zacharias, N., Finch, C. T., Girard, T. M., et al. 2013, AJ, 145, 44
Zacharias, N., Monet, D. G., Levine, S. E., et al. 2005, yCat, 1297, 0
Zickgraf, F.-J., Krautter, J., Reffert, S., et al. 2005, A&A, 433, 151
Zuckerman, B., & Song, I. 2004, ARA&A, 42, 685
Zuckerman, B., Song, I., Bessell, M. S., & Webb, R. A. 2001a, ApJL, 562, L87
Zuckerman, B., Song, I., & Webb, R. A. 2001b, ApJ, 559, 388
Zuckerman, B., & Webb, R. A. 2000, ApJ, 535, 959
Zuckerman, B., Webb, R. A., Schwartz, M., & Becklin, E. E. 2001c, ApJL, 549, L233
Zwitter, T., Siebert, A., Munari, U., et al. 2008, AJ, 136, 421